Penerbit Akademia Baru

Journal of Advanced Research in Micro and Nano Engineering

Journal homepage:
https://www.akademiabaru.com/submit/index.php/armne/index
ISSN: 2756-8210

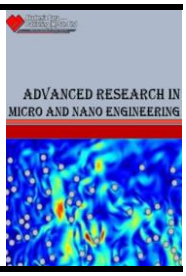

Superhydrophobic Surface of Ti6Al4V using Direct Nanosecond Laser Texturing

Mohd Harizan Zul[1], Mahadzir Ishak[1,*], Aiman Mohd Halil[1], Ramdziah Md Nasir[2], Moinuddin Mohammed Quazi[1]

[1] Joining, Welding and Laser Processing Lab, Faculty of Mechanical and Automotive Engineering Technology, Universiti Malaysia Pahang, 26600 Pekan, Pahang, Malaysia
[2] School of Mechanical Engineering, Engineering Campus, Universiti Sains Malaysia, 14300 Nibong Tebal, Penang, Malaysia

ARTICLE INFO

Article history:
Received 21 December 2023
Received in revised form 14 January 2024
Accepted 15 February 2024
Available online 30 March 2024

Keywords:
Ti6Al4V; laser texturing; wetting behaviour; superhydrophobic

ABSTRACT

This study aims to investigate the impact of laser parameters, including laser power, laser frequency, laser scan speed, and hatches line distance, on Ti6Al4V to create superhydrophobic surfaces. Surface profile and roughness play vital roles in achieving superhydrophobicity, and existing laser surface modification methods are time-consuming and lack subsequent steps for optimizing desired characteristics. A factorial design was implemented, varying laser power (12 and 18 W), laser frequency (40 and 60 kHz), laser scan speed (180 and 220 mm/s), and hatch line distance (0.25 and 0.45 mm). Surface morphology and topological properties were analyzed for surface characterization. The results demonstrate a significant increase in surface roughness profiles such as Sa and Sq by 6 and 5 times, respectively, compared to the untextured surface. These modifications also led to enhancements in surface topological properties. Regression analysis revealed the importance of controlling the surface profile for achieving superhydrophobicity. Statistical analysis indicated that laser power, laser frequency, and laser speed were the most significant parameters contributing to superhydrophobicity. The optimum laser parameters for superhydrophobic surfaces were determined as 18 W laser power, 40 kHz laser frequency, and 220 mm/s laser scan speed. In conclusion, this study emphasizes the critical role of surface topological properties in creating superhydrophobic surfaces on Ti6Al4V. Laser texturing techniques successfully improved surface roughness and profile, facilitating the development of superhydrophobic surfaces. These findings offer valuable insights for advancing surface engineering, with potential applications in the aerospace, automotive, and biomedical industries.

1. Introduction

Superhydrophobic surfaces (SHS), characterized by their extreme water repellency, have garnered significant attention in various fields due to their unique properties and potential applications [1]. The wetting surface characteristics are measured by the water contact angle (WCA). SHS exhibit WCA

* *Corresponding author.*
E-mail address: mahadzir@ump.edu.my

https://doi.org/10.37934/armne.17.1.117132

greater than 150°, along with low contact angle hysteresis [2], resulting in self-cleaning properties [3] and reduced drag [4]. The WCA below 150° and larger than 90° was assigned as hydrophobic (HS). Superhydrophobicity has found applications in areas such as anti-fouling coatings, corrosion resistance, microfluidics, and biomedical devices. Achieving SHS relies heavily on surface roughness and profile, which play crucial roles in altering the surface's wetting behavior [2,5]. However, achieving and maintaining such surfaces poses significant challenges in terms of fabrication, durability, and scalability.

Ti6Al4V, a titanium alloy, possesses exceptional mechanical properties, a high strength-to-weight ratio, and excellent corrosion resistance, making it widely used in various industries, including aircraft [6], automotive [7], and medical [8]. However, the native surface of Ti6Al4V material exhibits high wettability, leading to a tendency to attract and retain water droplets. According to Dou *et al.,* [9], the Ti alloy's water contact angle prior to laser irradiation was roughly 61.5 degrees, while Vanithakumari *et al*., [10] discovered that laser-patterned titanium samples were also hydrophilic immediately after patterning. As a consequence of this phenomenon, its potential applications in areas where superhydrophobicity is sought-after are impeded. Addressing this issue is crucial to expanding the potential applications of Ti6Al4V in industries where superhydrophobic properties can offer benefits like self-cleaning [9,11,12], reduced drag [13], and improved corrosion resistance [14].

Creating superhydrophobic surfaces on Ti6Al4V is challenging and requires specialized surface modification techniques to achieve the desired water-repellent properties. Exploiting the inherent advantages of Ti6Al4V, researchers have focused on creating superhydrophobic surfaces on this material. However, challenges remain due to the need for surface modification techniques that can achieve the desired roughness and profile without compromising the material's properties. Laser texturing has emerged as a promising method for surface modification of Ti6Al4V, offering precise control over surface features and enabling the creation of superhydrophobic surfaces [15].

Laser texturing is a surface modification technique that utilizes the high energy of laser beams to induce controlled structural changes on the material surface [16]. The process involves the localized melting and vaporization of the material, resulting in the formation of micro- and nanostructures [3]. Nanosecond lasers are advantageous for laser texturing due to their ability to generate high peak power and deliver energy pulses with a duration in the nanosecond range. This enables rapid energy transfer to the material surface, minimizing heat diffusion and associated thermal effects [17]. Moreover, nanosecond lasers offer flexibility in controlling laser parameters, such as power density and scanning speed, allowing precise control over the surface texture.

The main objective of this study is to contribute to the understanding of laser texturing as a viable technique for fabricating superhydrophobic surfaces on Ti6Al4V. After laser texturing, the surface characterization of the material such as surface morphology and topological properties is performed and well discussed to understand the effects of laser texturing on the material's surface features. The results of this experiment reveal a statistical summary and analysis of the effect of hatches line distance on the center-to-center diameter of the crater profile in comparison to laser speed, laser frequency, and laser power. The relationship between water contact angle and laser parameters is investigated to provide insights into the wetting behavior of laser-textured Ti6Al4V surfaces.

2. Experimental Procedures

2.1 Material

The material used in the experiment was the titanium alloy Ti6Al4V (Table 1 shows the chemical composition of this material). The specimens had dimensions of 5mm x 5mm x 1.2mm thickness. The specimens were cleaned using an ultrasonic acetone bath to remove any contaminants. After the

cleaning process, the specimens were blown with an air gun to remove excess liquid and were left to naturally dry.

Table 1
Nominal chemical composition of Ti6Al4V (wt. %)

Element	Ti	Al	V	O	C
Wt%	87.45±1.98	5.25±0.24	4.62±0.72	1.76±0.29	0.92±0.05

2.2 Laser Texturing

Laser texturing was performed using an IPG YLP series laser (from the UK) with a wavelength of 1064nm. The laser specification for laser texturing was as specified in Table 2. The laser parameters used in this study were determined based on experiments conducted using a one-factor-at-a-time approach. The experiment employed a factorial design with 4 factors and 2 levels, resulting in a total of 16 samples, as shown in Table 3. An ANOVA analysis was conducted, and the optimization process was carried out using Minitab software.

Table 2
Specifications of the laser marking system

Laser parameter	Unit	Value
Output power	W	0 – 30
Laser pulse frequency	kHz	20 – 200
Laser spot size	µm	30
Laser moving speed	mm/s	0 – 7,000

Table 3
Laser texturing parameters

Run	Laser power, W	Laser frequency, kHz	Laser scan speed, mm/s	Hatches line distance, mm
1	12	40	180	0.25
2	18	40	180	0.25
3	12	60	180	0.25
4	18	60	180	0.25
5	12	40	220	0.25
6	18	40	220	0.25
7	12	60	220	0.25
8	18	60	220	0.25
9	12	40	180	0.45
10	18	40	180	0.45
11	12	60	180	0.45
12	18	60	180	0.45
13	12	40	220	0.45
14	18	40	220	0.45
15	12	60	220	0.45
16	18	60	220	0.45

2.3 Surface Characteristics

Surface characterization was performed to evaluate the surface morphology and surface topological properties of the laser-textured surfaces. For surface morphology analysis, scanning electron microscopy (SEM) combined with energy-dispersive X-ray spectroscopy (EDX) was carried out using a JEOL, JSM-IT200. The surface topology and roughness profile were measured using a 3D

laser scan (Olympus LEXT 5000 series) surface profilometer with a magnification of 5 to 20 times. The main roughness parameters were the arithmetic average height (Sa) and root mean square height (Sq) values of 3D areal roughness parameters taken from the study by Romano *et al.,* [1], which have been calculated at three distinct places. The initial surface roughness for the as-received material is shown in Table 4.

Table 4
The roughness profile for as received sample

Sample	Sa (µm)	Sq (µm)
As received	0.591	0.744

In addition, cross-sectional form measurement was utilized to analyze the texture's shape, size, homogeneity, and density. The roughness factor or area ratio (r_w) for each textured surface configuration has been calculated as per Eq. (1) [8]

$$r_w = \frac{c^2 + \pi Dh}{c^2} \tag{1}$$

indicates experimentally determined geometrical parameters including texture depth (h), dimension (D), and texture center distance (c). The area ratio (r_w) was determined by averaging these measured values. The r_w values were altered in accordance with surface modifications in texture diameter, height, and center distance.

2.4 Wettability Test

Prior to the water contact angle (WCA) measurement, the surface was cleaned with acetone to ensure the absence of any residues. The wettability of the textured surfaces was evaluated using a contact angle tester. The test was conducted with deionized (DI) water, and a drop of 20 µl was placed on the surface. Five measurements were taken at different points on each specimen to obtain representative data.

3. Result and Discussion

3.1 Surface Characteristics

Micro cross groove surfaces with crater profiles of various sizes have been successfully fabricated on Ti6Al4V surfaces via laser texturing. Figure 1 shows experimentally measured geometrical parameters of h, D, and *c*. The created textures are homogeneous, of good size and shape, and defect-free, as shown in Figure 1(a). The laser parameters give effect to the various sizes of surface profile parameters indicated in Figure 1(b).

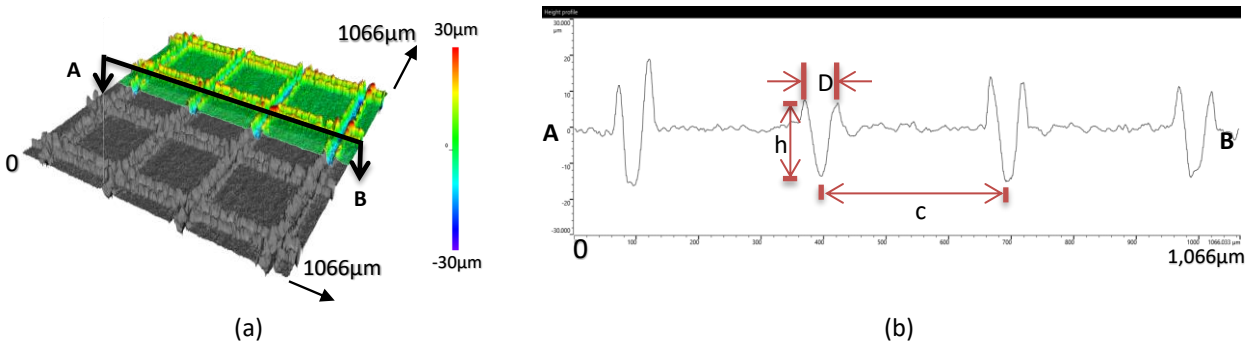

(a) (b)

Fig. 1. The laser textured surface measured by 3D laser scan (a) the laser textured surface with height profile (coloured) and intensity profile (grey); and (b) the surface height parameters profile of *c*, *D,* and *h* from cross-sectional AB

Table 5 provides a summary of regression statistics for the surface profile parameters (*c*, *D*, and *h*). The *P-value*s related to the parameters of the surface profile reflect the statistical significance of their association with the WCA. The Multiple-R is the value of the correlation coefficient between the profile parameters and the WCA. The R-square value is the proportion of the variance in the WCA that can be explained by the parameters *c*, *D*, and *h*. The Adjusted R-square adjusts the R-square value by the number of WCA and the sample size. These statistics suggest that the surface profile parameters have a substantial influence on WCA.

Table 5
Summary of regression statistics between surface profile parameters with the WCA

Profile	*c*	*D*	*h*
P-value	6.35×10^{-14}	1.32×10^{-6}	4.08×10^{-3}
Multiple-R	0.99858	0.96886	0.85173
R-square	0.99716	0.93870	0.72544
Adjusted R-square	0.99613	0.91640	0.62560

Figure 2 illustrates the significant value for each laser parameter based on the *P-value* of the surface profile parameters from the ANOVA. These microstructures' scale grooves enhance the surface area, which will aid in enhancing surface characteristics and diverse surface functional responses, such as wetting behavior. Consequently, all the surface profile parameter values (*c, D*, and *h*) were modified. The roughness factor is an important part of surface design and optimization [18]. In the next sections, therefore, the surface attributes associated with the roughness factor will be explored in detail.

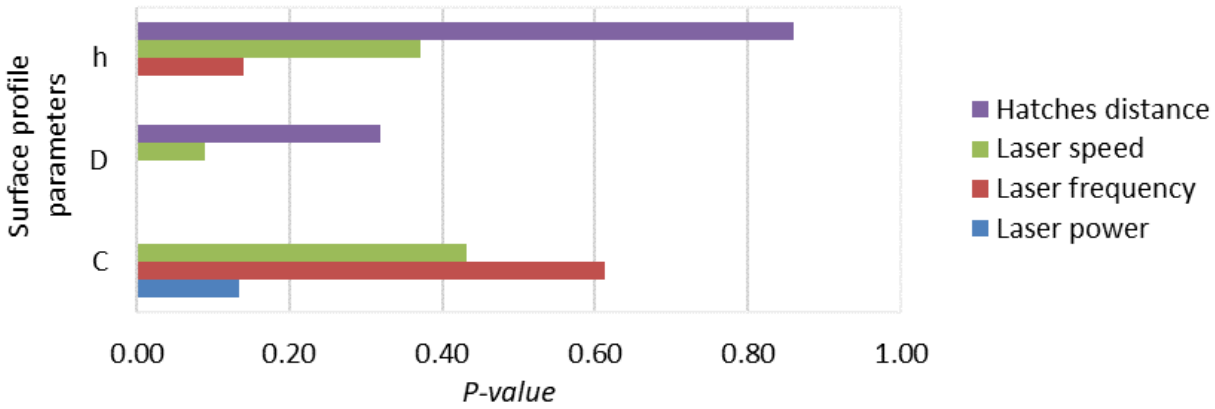

Fig. 2. The significant value of each laser parameter based on surface profile parameters

For the *h* profile, the least significant laser parameter is the hatches distance, while the most significant laser parameter is laser power. Laser power plays a crucial role in determining the energy input and heat generation during the process, resulting in enhanced melting and vaporization effects [17]. This leads to increased material removal and a greater depth of laser-induced features on the surface [16]. Conversely, laser speed and frequency primarily influence the spatial distribution and density of surface modifications. While laser power has a direct impact on profile formation, changes in laser speed and frequency primarily affect the lateral dimensions and arrangement of features.

The significant effect of laser power and laser frequency on the diameter, D, of the crater profile, compared to laser speed, can be attributed to the fundamental principles of laser-material interaction [19]. Higher laser power levels result in increased energy input and material removal, leading to a larger crater diameter [16]. The increase in energy input with higher laser power is a result of the greater amount of energy being delivered to the material's surface per unit of time [20]. Mathematically, the energy input, E, can be calculated as in Eq. (2) by multiplying the laser power, P, by the time, *t*, for which the laser is active.

$$E = P \times t \tag{2}$$

Laser power, P, refers to the rate at which energy is emitted by the laser source. When the laser power is increased, the laser emits more energy in each time period. This higher energy input affects laser-material interactions, including melting, vaporization, and ablation, affecting material processing results like material removal and surface alterations like crater diameter [21].

Laser frequency influences the temporal distribution of energy deposition on the surface. However, this is also the combined result of laser power, as reducing the peak power will reduce the laser energy input during the process. A low energy supply will result in less material removal from the surface [22]. In this study, higher laser frequencies resulting in more localized energy produced smaller crater diameters. Laser speed primarily affects the lateral dimensions and arrangement of features, but its impact on crater diameter is relatively less significant [23].

The hatches line distance determines the spacing between adjacent laser scan lines, *c* during the texturing process as displayed in Figure 3. A smaller hatch line distance as shown in Figure 3(b) leads to a denser arrangement of laser-induced features, resulting in a smaller center-to-center distance of the craters [23].

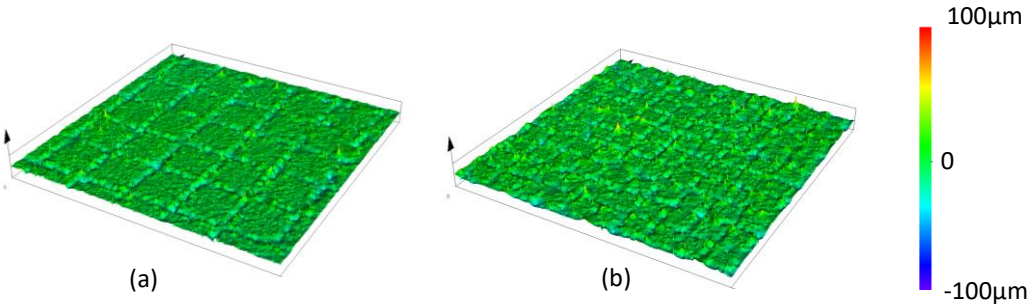

Fig. 3. The hatching line distance parameters of (a) 0.45mm, and (b) 0.25mm, between lines. The size of both image areas is 2,565.98µm x 2,572.497µm

Sa and Sq values of area surface roughness have grown dramatically for untextured surfaces (r_w = 1). Figure 4 depicts the statistical outcome of the relationship between r_w and Sa and Sq for all samples. The increase in surface roughness values of textured surfaces is attributable to the form of textures with more valleys and peaks resulting in form waviness [8]. Eq. (3) predicts that raising the

values of *D* and *h* and creating a crater along the laser scanning groove will increase r_w.

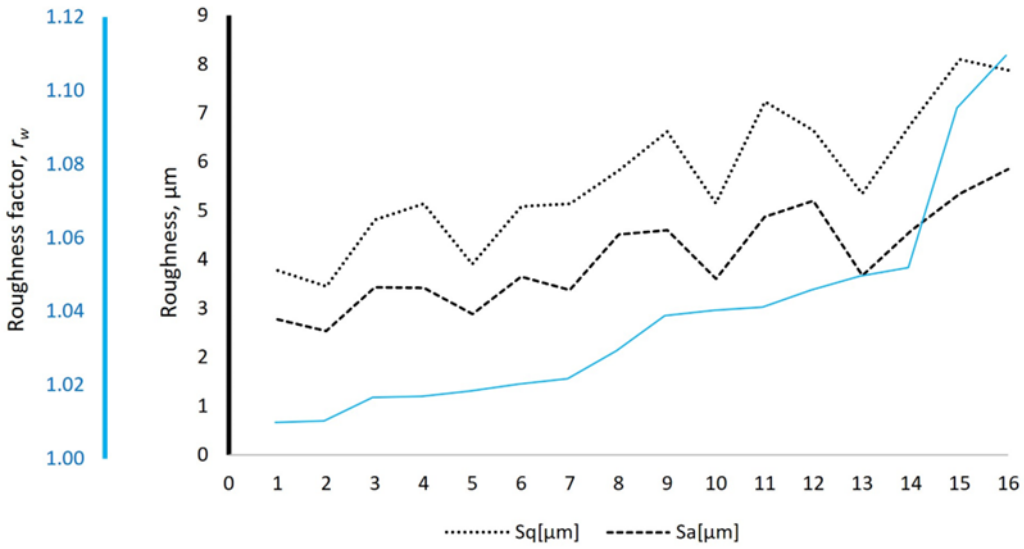

Fig. 4. The comparison between the roughness factor,r_w with the values of surface roughness profile Sa and Sq parameter

As illustrated in Figure 5, the chemical composition and EDS spectrum of created textured surfaces are dramatically altered, indicating that the approach impacts the chemical composition of the surfaces. Similar to the work that had been done by Ahuir-Torres *et al.,* [16], the results indicate that C and O have an effect on the surface morphological properties following laser texturing. These results will be elaborated upon in the subsequent section.

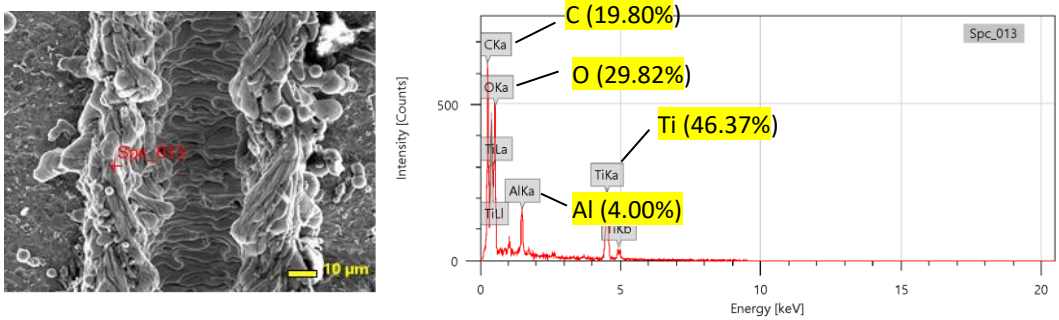

(a) (b)

Fig. 5. The elemental composition of the laser textured surface

3.2 Factorial Regression Analysis

3.2.1 ANOVA results

The result of the water contact angle was analyzed using regression statistics based on ANOVA and response optimizer via Minitab software. Initially, the result was tested by using a probability plot for normal distribution before further statistical analyses and conclusions as displayed in Figure 6. The regression analysis revealed that the Multiple-R-value was 0.8333, indicating a moderately strong positive correlation between the independent and dependent variables as shown in Table 6. The R-square value was 0.6944, indicating that approximately 69.44% of the variance in the dependent variable was explained by the independent variables. The adjusted R-square value of 0.5833

suggested that around 58.33% of the variance in the dependent variable was accounted for while considering the complexity of the model. The standard error was 5.0413, representing the average deviation between the observed and predicted values. A sample size of 16 observations was used in the analysis. Overall, the results indicated a significant relationship between the variables, with the regression model providing a reasonably accurate estimation of the dependent variable.

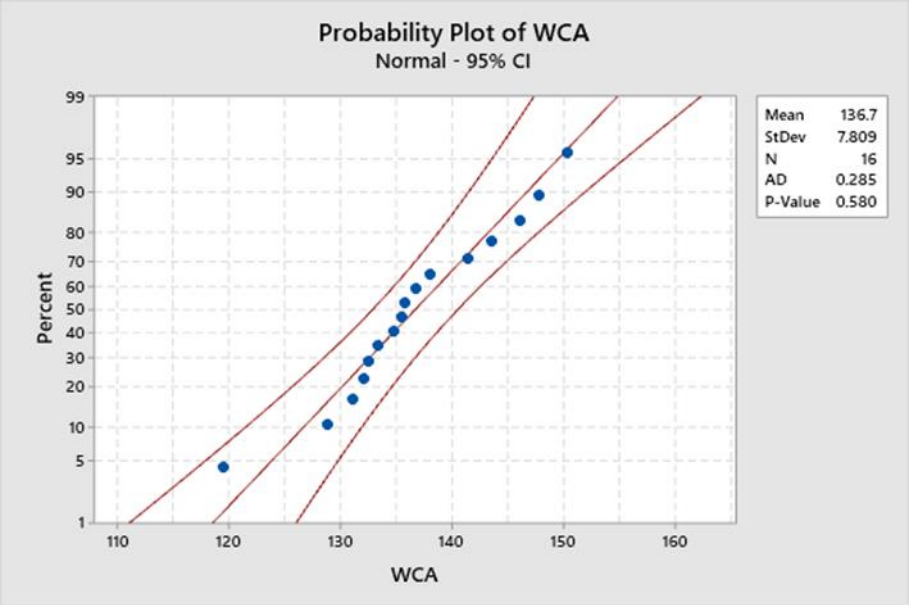

Fig. 6. Normal distribution plot from 16 observations

Table 6
Summary output from regression statistics

Multiple-R	0.8333
R-square	0.6944
Adjusted R-square	0.5833
Standard Error	5.0413
Observations	16

Multiple linear regression was calculated to predict water contact angle based on main laser parameters such as laser power, laser scan frequency, laser scan speed, and the scanning line hatches. Based on Table 7 (model summary and ANOVA), a significant regression equation was found (F (4,11) = 6.25, p<0.007), with an R^2 of 0.6944. Wetting surface behaviour is predicted by following Eq. (3)

$$\text{WCA}=106.1 + 0.379(\text{laser power}) - 0.403(\text{laser frequency}) + 0.1458(\text{laser scan speed}) + 7.6(\text{hatches line distance}) \quad (3)$$

where the independent variables are coded as in Table 7. WCA increased by 0.38° for each Watt of laser power, decreased by 0.40° for each kHz of a laser scan frequency, increased by 0.15° for each mm/s of a laser scan speed, and increased by 7.63° more than the smaller hatch. Based on Figure 7, laser power, laser scan frequency, and laser scan speed were significant predictors at the $p < 0.05$ level, for the fabrication of superhydrophobic.

Table 7
ANOVA table

	df	SS	MS	F	*P-value*
Regression	4	635.2322	158.8081	6.24858	0.0071
Residual	11	279.5658	2.41508		
Total	15	914.798			

Summary of coefficients

	Coefficients	*P-value*
Intercept	106.1011	3.9229×10^{-5}
Laser power	0.38	0.0200
Laser frequency	-0.40	0.0084
Laser scan speed	0.15	0.0410
Hatches distance	7.63	0.5575

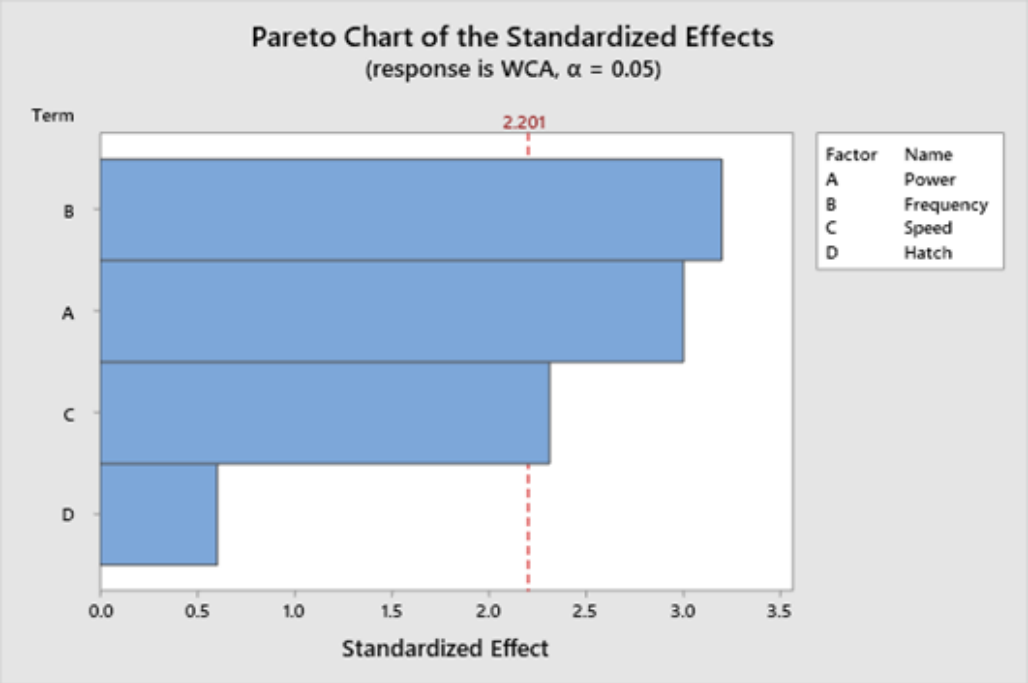

Fig. 7. Pareto plot of effects from the experiment

3.2.2 Parameter plot-effect

The Minitab software system was used to analyze the data. The first objective was to understand what factors affect the WCA. A main effects plot was constructed as depicted in Figure 8. The Pareto chart plot in the previous figure clearly indicated that factors B, A, and C, in that order, are the most important ones. Factor D has no impact on the WCA. This factor can be set at its most appropriate distance level (in this case the high level). The main effects plot also tells us that factor A must be kept at its high level for higher energy density for huge material removal and high depth [24], and factor B must be kept at its low level because lower frequencies result in less localized energy and producing larger crater diameters [25]. A high level of factor C will affect the lateral dimensions and arrangement of features [26].

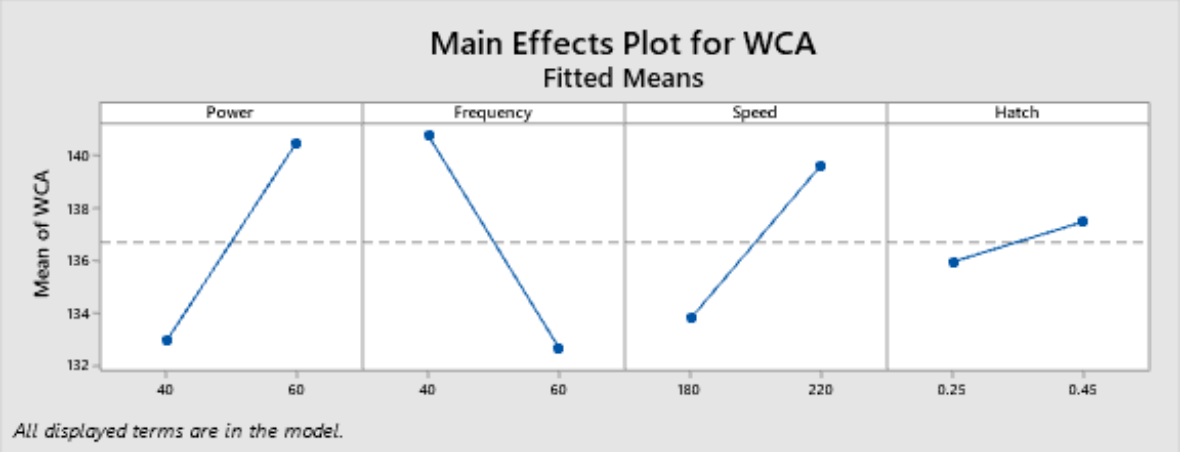

Fig. 8. Main plot of effects from the experiment

Figure 9 shows the interactions among the factors. The results demonstrate a strong relationship between laser power and both laser frequency and speed. The higher laser power directly affects laser frequency and speed, leading to an increased WCA [18]. However, the contact angle does not change substantially at different nanosecond laser processing speeds. This comparable result was achieved by Li *et al.,* [3] showing that when the laser processing speed increases, the contact angle decreases. Meanwhile, the results from Figure 7 indicate that the parameter manipulated by the hatch line distance is not highly significant. However, a hatching distance of 0.45mm was found to increase the water contact angle (WCA).

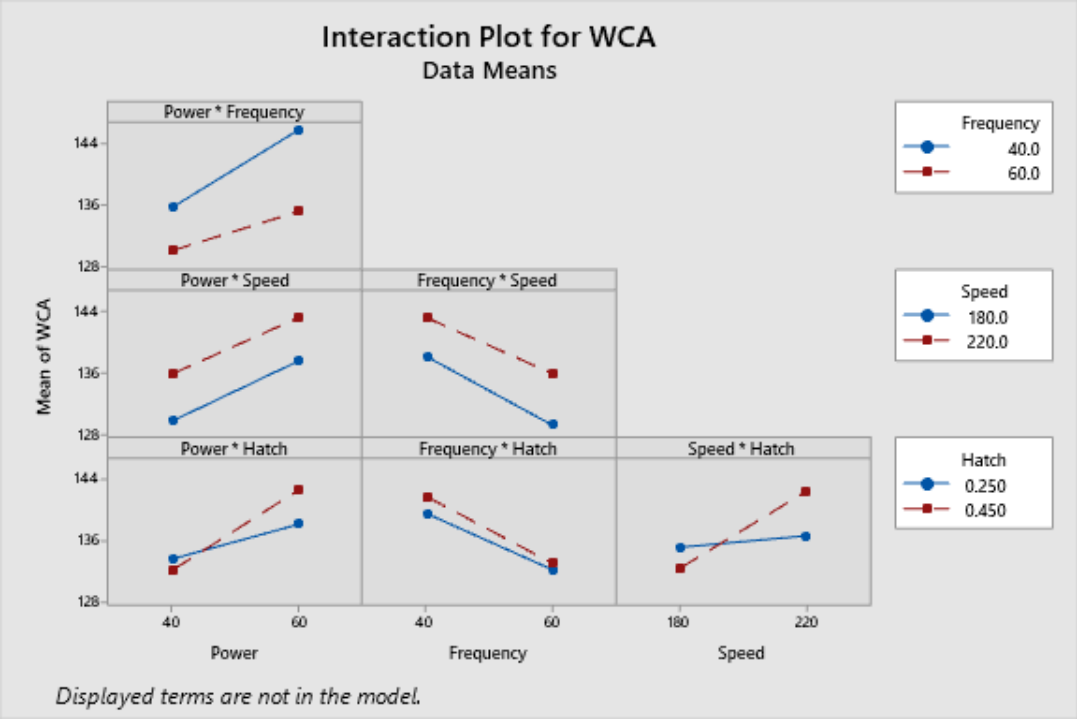

Fig. 9. Plot of interaction via Minitab

3.2.3 Response optimization

Minitab has a new feature that allows users to optimize a response variable based on specified constraints and objectives. Figure 10 shows the optimized value of different laser parameters with

the help of a response optimizer via Minitab. It is observed that the optimized value to achieve high WCA as shown in Figure 10(a) indicates the superhydrophobic surface (SHS) is laser power of 18W, laser scan frequency of 40 kHz, laser scan speed of 220 mm/s, and 0.450 mm line hatching distance. On the other hand, the hydrophobic surface (HS) is set to the lowest WCA as shown in Figure 10(b) which is the combination of the 12W, 60 kHz, and 180 mm/s with the line hatching distance maintained at 0.450 mm. Table 8 shows the results for the prediction and actual value for both surface-wetting properties. For the SHS sample, the predicted value is 148.193°, while the actual value is 150.326°, resulting in an error of 1.4%. For the HS sample, the predicted value is 125.193°, and the actual value is 129.437°, with an error of 3.2%. The error percentages provide a measure of the deviation between the predicted and actual values, indicating the accuracy of the predictions. In this case, both the SHS and HS conditions have relatively low error percentages, suggesting that the predicted values closely align with the actual values.

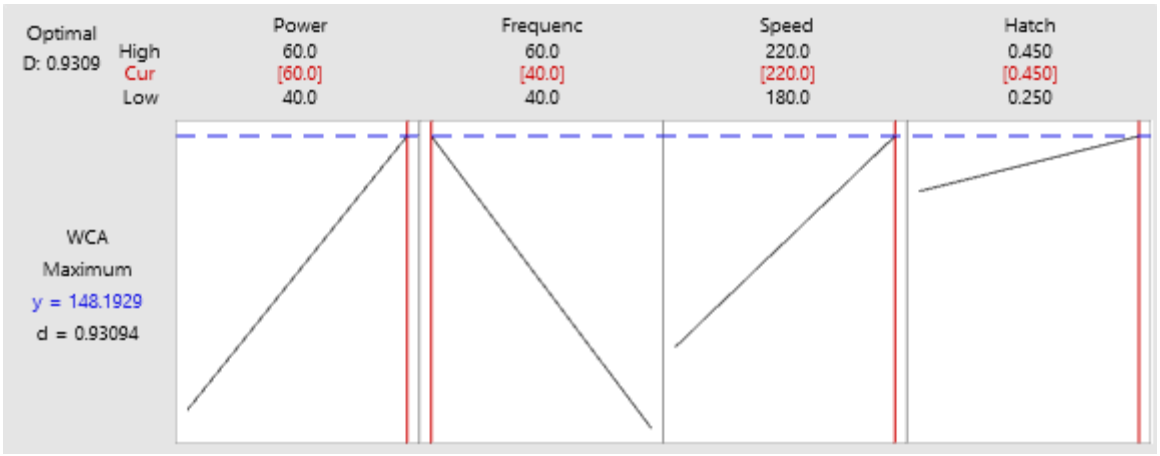

(a)

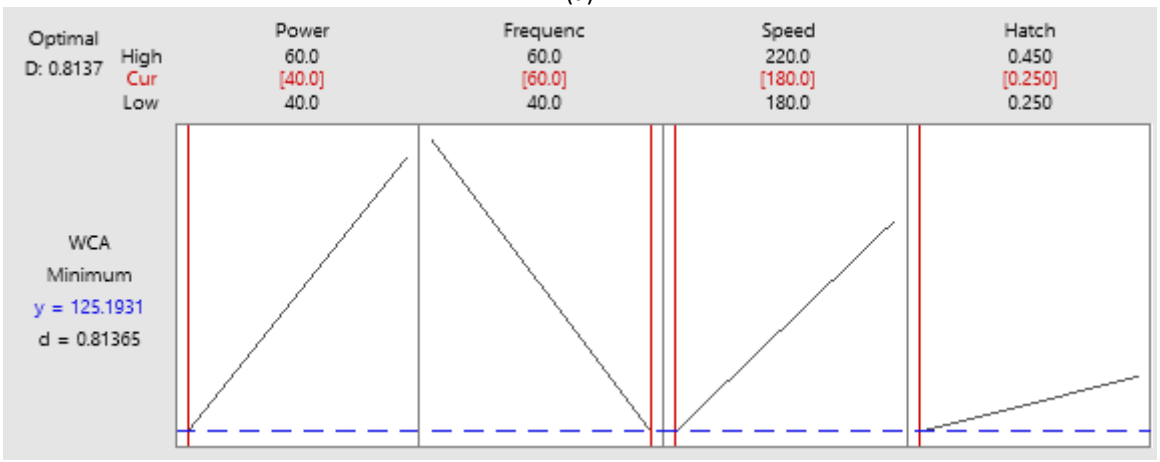

(b)

Fig. 10. Response optimizer via Minitab software for (a) prediction for SHS, and (b) prediction value for HS

Table 8
The value of WCA from software prediction and actual measurements

Surface (ID)	Predict value	Actual value	Error, %
Untextured surface (UTS)	N/A	~ 80	N/A
SHS	148.193	150.326	1.4
HS	125.193	129.174	3.2

3.3 Analysis of Textured Surface on Wetting Behaviour

To comprehend the mechanisms underlying the wetting of liquids on solid surfaces, models of wetting behaviour have been constructed as displayed in Figure 11. The Young-Laplace equation represents the balance of forces acting on the three-phase contact line, where the contact angle is determined by the surface tension and pressure difference across the contact line [27]. The Wenzel model is used to describe the behaviour of liquids on smooth surfaces in which the liquid completely wets the surface, resulting in an increase in the contact area and a decrease in apparent contact angle [28]. The Cassie-Baxter model is used to describe the behaviour of liquid droplets on rough surfaces, where the liquid only wets the tops of the roughness features, resulting in a decreased contact area and an increased apparent contact angle [29].

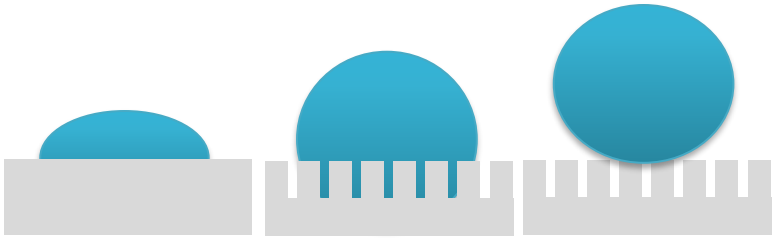

(b) (b) (c)

Fig. 11. The wetting model of (a) Young model, (b) Wenzel model, and (c) Cassie-Baxter model

Prior to laser ablation, the raw Titanium surface was hydrophilic, as its WCA was around 80 degrees. Immediately after laser processing, the surfaces of all samples exhibited superhydrophilicity, and the droplet was able to fully spread out and penetrate the groove ablated by the laser. The occurrence is consistent with that described in the prior literature and is explicable by Wenzel's Eq. (4) [28]

$$\cos \theta_w = r_w \cos \theta_0 \tag{4}$$

where r_w>1 is the roughness factor, θ_w and θ_0 are the contact angle on the rough surface and the ideally smooth surface, respectively. It was stated that the textured metallic surface got increasingly hydrophobic and eventually superhydrophobic with time and air exposure. This is the result of a chemical reaction between the surface and some airborne components, including carbon and oxygen (refer to Figure 5). Li *et al.,* [3] revealed that the breakdown of CO_2 continues to be slow over time and that non-polar carbon accumulates on rough surfaces. Thus, the initial hydrophilic surface of a microstructure that has been laser-treated can be transformed into a superhydrophobic surface [30].

In this study, after laser texturing, two sets of the laser textured surface were cleaned by ultrasonic with an acetone bath, and kept the sample in an open-air environment for 24 hours. Within one day, most of the sample surfaces achieved the shift from hydrophilic to hydrophobic. Figure 12 shows the apparent WCA for all samples. Firstly, the WCAs increased for the sample with higher r_w. As discussed earlier, r_w depends on the surface profile parameter and also the roughness parameter of Sa and Sq. In conclusion, the surface area roughness parameter of Sa and Sq proved to have an effect on the SHS fabrication. On the other hand, the value of the surface contact angle is also affected by the state of the droplet on the surface.

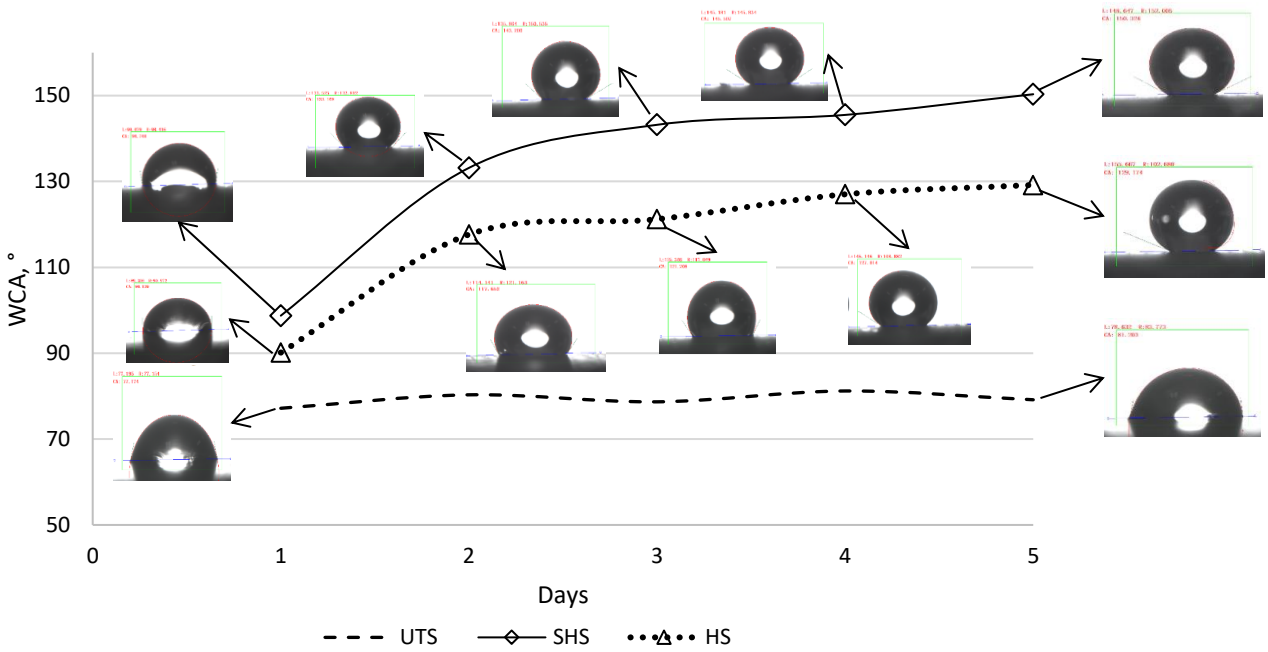

Fig. 12. Wetting behaviour of untextured surface and laser textured surface of Ti6Al4V for 5 days

To improve the hydrophobicity of a surface, a stable Cassie-Baxter condition is required. The surface contact angle at the Cassie-Baxter state is represented by the following Eq. (5)

$$\cos\,\theta_{CB} = f(1+r_f\,\cos\theta_0)-1 \tag{3}$$

where f is the fraction of solid surface area wet by the liquid in total apparent area, r_f is the roughness ratio of the wetted surface. Statistically, the Sa and Sq values increased by 5 and 6 times for SHS as compared to the untextured surface. The increment in the area ratio value increased by 5%, indicating that the area surface roughness value also increased as shown in Figure 13, the roughness of the SHS surface more significant.

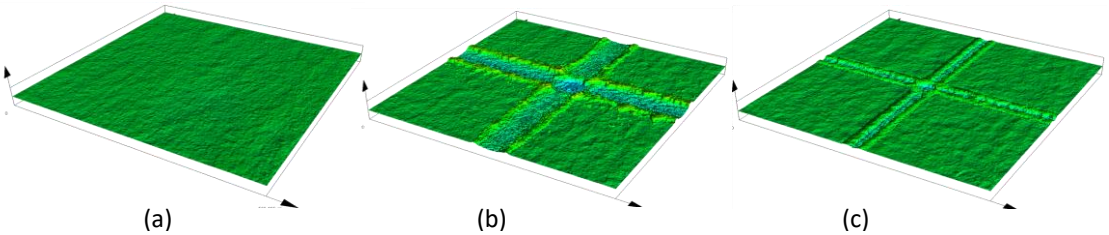

Fig. 13. The surface profile of (a) UTS, (b) SHS characteristics, and (c) HS characteristics

After the laser ablation, the condensation of the molten material around the scanning route generated certain elevated frames. The textured surface does not need to be extremely rough; however, it should be designed to encourage air trapping [5]. In this experiment, when the laser power is set to 12W, the surfaces can achieve hydrophobicity as displayed in Figure 14(b). When the height of the convex from crater creation is appropriate, the liquid is unable to enter the surface's groove, therefore the water droplet was supported by the raised frames, and air pockets developed between the water drop and the rough surface [19,31], which displayed the Cassie-Baxter condition as illustrated in Figure 14(c). The laser power and laser frequency influenced the frame's height and width, whereas the side length of the grid pattern influenced the values of D and h. In Figure 14(a),

however, no surface structures can support the droplet, and the droplet is stuck to the surface, exhibiting the Wenzel condition.

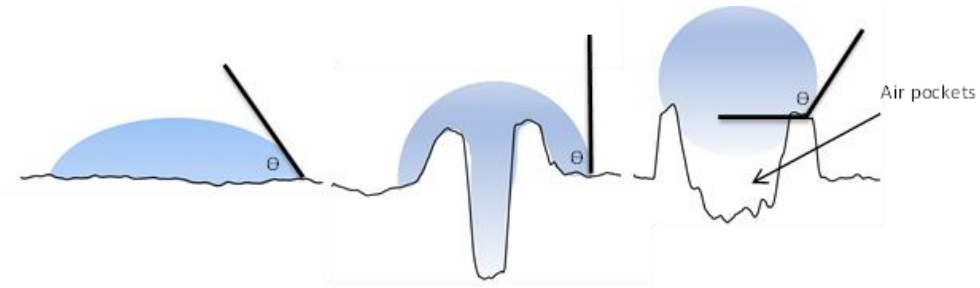

(a) (b) (c)

Fig. 14. The apparent WCA profile of the (a) untextured surface, (b) HS: *D*=32.86µm and *h*=20.18µm, and (c) SHS: *D*=74.13µm and *h*=32.60µm

In conclusion, wettability is a fundamental property that governs the behavior of liquids on solid surfaces. Wetting behavior models provide insights into the mechanisms involved in wetting, which can be useful in designing surfaces with specific wetting properties. Achieving superhydrophobic surfaces is of great interest in various applications, and there are various approaches to achieve this, such as surface roughness and surface chemistry modification.

4. Conclusion

In conclusion, this study demonstrates the significance of laser power, laser speed, laser frequency, and hatch line distance as critical parameters for the design and optimization of superhydrophobic surfaces. These parameters have been shown to influence surface profile formation, lateral dimensions, and water contact angle.

i Through the utilization of a response optimizer, the optimized values for the laser power of 18W, laser frequency of 40 kHz, laser speed of 220 mm/s, and 0.450 mm line hatching distance were determined for superhydrophobic surface fabrication. The predicted value is 148.193°, while the actual value is 150.326°, with an error of 1.4%. The error percentages provide a measure of the deviation between the predicted and actual values, indicating the accuracy of the predictions.

ii The study reveals that laser texturing can effectively transform hydrophilic surfaces into hydrophobic surfaces within a day, with the surface areal roughness parameters of Sa and Sq playing a role in superhydrophobicity. The interaction between the droplet state and the surface further impacts the contact angle.

iii The laser ablation process creates raised frames by the laser power is set to 12W, which, when appropriately sized, support water droplets and create air pockets between the droplet and rough surface, resulting in the Cassie-Baxter condition.

These findings contribute to the understanding and advancement of surface engineering for superhydrophobic applications.

Acknowledgments
The author would like to acknowledge University Malaysia Pahang al-Sultan Abdullah (UMPSA) for providing financial support under the Postgraduate Research Grant Scheme (PRGS200302) and the

facilities at the Joining, Welding, and Laser Processing (JWL) Lab at the Faculty of Mechanical and Automotive Engineering Technology and the Material Lab at the Faculty of Manufacturing and Mechatronic Engineering Technology, the Centre for Research in Advanced Fluid and Process (CARIFF), and also the Malaysian Public Services Department, Department of Prime Minister Office of Malaysia, which made this study possible.

References

[1] Romano, Jean-Michel, Mert Gulcur, Antonio Garcia-Giron, Elena Martinez-Solanas, Ben R. Whiteside, and Stefan S. Dimov. "Mechanical durability of hydrophobic surfaces fabricated by injection moulding of laser-induced textures." *Applied Surface Science* 476 (2019): 850-860. https://doi.org/10.1016/j.apsusc.2019.01.162

[2] Liu, Ri, Zhendong Chi, Liang Cao, Zhankun Weng, Lu Wang, Li Li, Sadaf Saeed, Zhongxu Lian, and Zuobin Wang. "Fabrication of biomimetic superhydrophobic and anti-icing Ti6Al4V alloy surfaces by direct laser interference lithography and hydrothermal treatment." *Applied Surface Science* 534 (2020): 147576. https://doi.org/10.1016/j.apsusc.2020.147576

[3] Li, Jiaru, Jinkai Xu, Zhongxu Lian, Zhanjiang Yu, and Huadong Yu. "Fabrication of antireflection surfaces with superhydrophobic property for titanium alloy by nanosecond laser irradiation." *Optics & Laser Technology* 126 (2020): 106129. https://doi.org/10.1016/j.optlastec.2020.106129

[4] Knights, Michael J., Roy Donald, Diego Galletta, Pun Kul, and Faik A. Hamad. "Experimental Analysis of The Effect of Hydrophobic Coating on Pressure Drop in Small Pipes." *Journal of Advanced Research in Fluid Mechanics and Thermal Sciences* 77, no. 1 (2021): 24-35. https://doi.org/10.37934/arfmts.77.1.2435

[5] Nosonovsky, Michael, and Bharat Bhushan. "Hierarchical roughness optimization for biomimetic superhydrophobic surfaces." *Ultramicroscopy* 107, no. 10-11 (2007): 969-979. https://doi.org/10.1016/j.ultramic.2007.04.011

[6] Hussin, Amil Hamja Ali, Shamsul Sarip, and Mohd Khairi Abu Husain. "Investigation of Ultrasonic-Assisted Drilling (UAD) Parameters For Hole Making Of Ti-6Al-4V Using Taguchi Method." *Journal of Advanced Research in Applied Sciences and Engineering Technology* 27, no. 1 (2022): 45-61. https://doi.org/10.37934/araset.27.1.4561

[7] Schauerte, Oliver. "Titanium in automotive production." *Advanced engineering materials* 5, no. 6 (2003): 411-418. https://doi.org/10.1002/adem.200310094

[8] Jain, Ankit, and Vivek Bajpai. "Alteration in Ti6Al4V implant surface properties with micro textures density." *Surface Engineering* 38, no. 2 (2022): 174-182. https://doi.org/10.1080/02670844.2022.2058163

[9] Dou, Hong-qiang, Hao Liu, Shizhen Xu, Yu Chen, Xinxiang Miao, Haibing Lü, and Xiaodong Jiang. "Influence of laser fluences and scan speeds on the morphologies and wetting properties of titanium alloy." *Optik* 224 (2020): 165443. https://doi.org/10.1016/j.ijleo.2020.165443

[10] Vanithakumari, S. C., Choubey Ambar Kumar, C. Thinaharan, Gupta Ram Kishor, R. P. George, R. Kaul, K. S. Bindra, and Philip John. "Laser patterned titanium surfaces with superior antibiofouling, superhydrophobicity, self-cleaning and durability: Role of line spacing." *Surface and Coatings Technology* 418 (2021): 127257. https://doi.org/10.1016/j.surfcoat.2021.127257

[11] TP, Rasitha, and John Philip. "Optimal condition for fabricating mechanically durable superhydrophobic titanium surface by rapid breakdown anodization: Self cleaning and bouncing characteristics." *Applied Surface Science* 585 (2022): 152628. https://doi.org/10.1016/j.apsusc.2022.152628

[12] Zhang, Xiao, Yi Wan, Bing Ren, Hongwei Wang, Mingzhi Yu, Anqi Liu, and Zhanqiang Liu. "Preparation of superhydrophobic surface on titanium alloy via micro-milling, anodic oxidation and fluorination." *Micromachines* 11, no. 3 (2020): 316. https://doi.org/10.3390/mi11030316

[13] Xin, Guoqiang, Congyi Wu, Haiyin Cao, Weinan Liu, Bo Li, Yu Huang, Youmin Rong, and Guojun Zhang. "Superhydrophobic TC4 alloy surface fabricated by laser micro-scanning to reduce adhesion and drag resistance." *Surface and Coatings Technology* 391 (2020): 125707. https://doi.org/10.1016/j.surfcoat.2020.125707

[14] Singh, Raghuvir, M. Martin, and N. B. Dahotre. "Influence of laser surface modification on corrosion behavior of stainless steel 316L and Ti–6Al–4V in simulated biofluid." *Surface engineering* 21, no. 4 (2005): 297-306. https://doi.org/10.1179/174329405X55320

[15] Sirdeshmukh, Neelesh, and Ganesh Dongre. "Achieving controlled topography and wettability through laser surface texturing of Ti6Al4V for bioengineering applications." *Results in Engineering* 17 (2023): 100898. https://doi.org/10.1016/j.rineng.2023.100898

[16] Ahuir-Torres, Juan Ignacio, M. A. Arenas, W. Perrie, and J. De Damborenea. "Influence of laser parameters in surface texturing of Ti6Al4V and AA2024-T3 alloys." *Optics and Lasers in Engineering* 103 (2018): 100-109. https://doi.org/10.1016/j.optlaseng.2017.12.004

[17] Sierra, D. Rico, S. P. Edwardson, and G. Dearden. "Laser surface texturing of titanium with thermal post-processing for improved wettability properties." *Procedia CIRP* 74 (2018): 362-366. https://doi.org/10.1016/j.procir.2018.08.143
[18] Al-Mahdy, A., H. R. Kotadia, M. C. Sharp, T. T. Opoz, J. Mullett, and J. I. Ahuir-Torres. "Effect of Surface Roughness on the Surface Texturing of 316 l Stainless Steel by Nanosecond Pulsed Laser." *Lasers in Manufacturing and Materials Processing* 10, no. 1 (2023): 141-164. https://doi.org/10.1007/s40516-022-00199-x
[19] Singh, Abhilasha, Divyansh Singh Patel, J. Ramkumar, and Kantesh Balani. "Single step laser surface texturing for enhancing contact angle and tribological properties." *The International Journal of Advanced Manufacturing Technology* 100 (2019): 1253-1267. https://doi.org/10.1007/s00170-018-1579-8
[20] Su, Yongsheng, Liang Li, Ning He, and Wei Zhao. "Experimental study of fiber laser surface texturing of polycrystalline diamond tools." *International Journal of Refractory Metals and Hard Materials* 45 (2014): 117-124. https://doi.org/10.1016/j.ijrmhm.2014.03.001
[21] Li, Xinxin, and Yingchun Guan. "Theoretical fundamentals of short pulse laser–metal interaction: A review." *Nanotechnology and Precision Engineering (NPE)* 3, no. 3 (2020): 105-125. https://doi.org/10.1016/j.npe.2020.08.001
[22] Zaifuddin, A. Q., MH AIMAN, MM QUAZI, Mahadzir Ishak, and J. Shamini. "Influence of Laser Surface Texturing (LST) Parameters on the Surface Characteristics of Ti6Al4V and the Effects Thereof on Laser Heating." *Lasers in Engineering (Old City Publishing)* 51, no. 6 (2021).
[23] Dongre, Ganesh, Avadhoot Rajurkar, Ravi Raut, and Sumit Jangam. "Preparation of super-hydrophobic textures by using nanosecond pulsed laser." *Materials Today: Proceedings* 42 (2021): 1145-1151. https://doi.org/10.1016/j.matpr.2020.12.497
[24] Vázquez Martínez, Juan Manuel, Jorge Salguero Gómez, Moises Batista Ponce, and Francisco Javier Botana Pedemonte. "Effects of laser processing parameters on texturized layer development and surface features of Ti6Al4V alloy samples." *Coatings* 8, no. 1 (2017): 6. https://doi.org/10.3390/coatings8010006
[25] Rafiee, Kimia, Homam Naffakh-Moosavy, and Elnaz Tamjid. "The effect of laser frequency on roughness, microstructure, cell viability and attachment of Ti6Al4V alloy." *Materials Science and Engineering: C* 109 (2020): 110637. https://doi.org/10.1016/j.msec.2020.110637
[26] Aziz, HM Tariq, A. Sen, G. Kibria, B. Doloi, and B. Bhattacharyya. "Parametric Analysis and Optimization of Surface Finish obtained during Microtexturing on Titanium using Pulsed Nd: YAG Laser." (2016).
[27] Gennes, Pierre-Gilles, Françoise Brochard-Wyart, and David Quéré. *Capillarity and wetting phenomena: drops, bubbles, pearls, waves*. Springer New York, 2004.
[28] Wenzel, Robert N. "Resistance of solid surfaces to wetting by water." *Industrial & engineering chemistry* 28, no. 8 (1936): 988-994. https://doi.org/10.1021/ie50320a024
[29] Cassie, A. B. D., and SJToTFS Baxter. "Wettability of porous surfaces." *Transactions of the Faraday society* 40 (1944): 546-551. https://doi.org/10.1039/tf9444000546
[30] Ijaola, Ahmed Olanrewaju, Emmanuel Anuoluwa Bamidele, Cletus John Akisin, Idris Temitope Bello, Abiola Tunde Oyatobo, Abdullah Abdulkareem, Peter Kayode Farayibi, and Eylem Asmatulu. "Wettability transition for laser textured surfaces: a comprehensive review." *Surfaces and Interfaces* 21 (2020): 100802. https://doi.org/10.1016/j.surfin.2020.100802
[31] Wang, Yutong, Changjun Ke, Tianhao Wu, Xiaoran Zhao, and Ran Wang. "Nanosecond laser texturing with hexagonal honeycomb micro-structure on Titanium for improved wettability and optical properties." *Optik* 192 (2019): 162953. https://doi.org/10.1016/j.ijleo.2019.162953